



HAL
open science

Playability of Self-Sustained Musical Instrument Models: Statistical Approaches

Martin Pégeot, Tom Colinot, Jean-Baptiste Doc, Vincent Fréour, Christophe
Vergez

► **To cite this version:**

Martin Pégeot, Tom Colinot, Jean-Baptiste Doc, Vincent Fréour, Christophe Vergez. Playability of Self-Sustained Musical Instrument Models: Statistical Approaches. 2024. hal-04777809v2

HAL Id: hal-04777809

<https://hal.science/hal-04777809v2>

Preprint submitted on 25 Nov 2024

HAL is a multi-disciplinary open access archive for the deposit and dissemination of scientific research documents, whether they are published or not. The documents may come from teaching and research institutions in France or abroad, or from public or private research centers.

L'archive ouverte pluridisciplinaire **HAL**, est destinée au dépôt et à la diffusion de documents scientifiques de niveau recherche, publiés ou non, émanant des établissements d'enseignement et de recherche français ou étrangers, des laboratoires publics ou privés.



Distributed under a Creative Commons Attribution 4.0 International License



Playability of self-sustained musical instrument models: statistical approaches

Martin Pégeot¹, Tom Colinot², Jean-Baptiste Doc³, Vincent Fréour⁴, and Christophe Vergez^{1,*}

¹ Aix Marseille Univ, CNRS, Centrale Med, LMA UMR7031, Marseille, France

² Buffet Crampon, Mantes-La-Ville, France

³ Laboratoire de Mécanique des Structures et Système Couplés, France

⁴ Yamaha Corporation, Research and Development Division, Hamamatsu, Japan

Received 1 March 2024, Accepted 25 October 2024

Abstract – Self-sustained musical instruments, such as wind or bowed string instruments, are complex nonlinear systems. They admit a wide variety of regimes, which sometimes coexist for certain values of the control parameters. This phenomenon is known as multistability. With fixed parameters, the selection of a regime and the shape of the transient depend not only on the values of the control parameters, but also on the initial conditions. In this article, we focus on the statistical influence of initial conditions on regime selection and transient duration. An existing sample-based method called basin stability is presented to calculate the probability of occurrence of each regime. A second sample-based method is proposed for the calculation of the probability density function of transient durations. Additionally, a study taking into account specific control scenarios is presented to highlight the influence of the distribution of initial conditions considered for the statistical methods. These methods are presented on a Van der Pol oscillator seen as a prototypical musical instrument model. They are then applied to a physical model of trumpet, to demonstrate their potential for a high dimensional self-oscillating musical instrument. Finally, their interest regarding questions of playability is discussed.

Keywords: Self-sustained musical instruments, Multistability, Basin stability, Transient duration, Playability

1 Introduction

Musical instruments are complex dynamical systems. Some of them are self-sustained oscillators, meaning that a continuous energy supply can make them oscillate. Wind instruments and bowed string instruments belong to this category. These instruments admit a wide variety of regimes, which sometimes coexist for certain values of control parameters. This is known as multistability. Multistability is a common phenomenon in self-sustained oscillators. It has been observed experimentally, theoretically and numerically on a wide variety of instruments, e.g., single and double reed instruments [1–3], flutes [4], brass instruments [5], vocal folds [6] and bowed string instruments [7]. There are multiple works focusing on mapping the operating regimes of these instruments [8]. We find in [9, 10] among the first curves representing the evolution of the amplitude of a solution as a function of a control parameter. The stability of these solutions is also studied few years later [11]. A seminal work of Dalmont et al. [12] represents bifurcation diagrams of self-sustained musical

instruments. These diagrams show the evolution of known solution properties as a function of one or more control parameters. The stability of these solutions is given, as well as some key features, such as amplitude and fundamental frequency for periodic solutions. Thanks to these diagrams, one can predict the behavior of an instrument whose control parameters vary in a quasi-static manner – i.e., slowly in relation to the system’s rate of evolution. In the case of multistability, bifurcation diagrams predict hysteretic behaviors, such as those of reed and brass instruments [13] or flute-like instruments [14]. Some unexpected regimes are also predicted with this method, such as the ghost note in brass instruments [15] or the wolf tone of the cello [16]. Nevertheless, it is much more difficult to predict the regime of a multistable instrument when the control parameters vary rapidly. In particular, the blowing pressure dynamics are shown to have an influence over the regime selection in flute-like instruments [17]. Similar results are shown in [18] for the saxophone.

Similarly, once the control parameters are fixed, the time required to reach the steady state depends on the previous evolution of the control parameters. This phenomenon was observed by [19, 20] on the clarinet. Generally

*Corresponding author: vergez@lma.cnrs-mrs.fr

speaking, the duration of attack transients [7, 21] or transitions between notes [22] are important topics, since the quality of a transient perceived by a musician or a listener depends greatly on its characteristics and duration [23]. The duration of the transients that gives rise to a sound is thus studied on multiple self-sustained instruments, from the trombone [24] to the cristal Baschet [25], using linear stability analysis. Like the prediction of the playing regime, the duration of the transient is estimated for control parameters varying in a quasi-static manner. Linear stability analysis cannot predict dynamic phenomena such as those observed by [19, 20]. Finally, despite their high efficiency in the quasi-static regime, current methods for analyzing self-oscillating instruments are limited when considering rapidly varying control parameters. By taking these rapid variations into account, the dimensionality of the problem becomes infinite since the parameters can follow any time series. Consequently, it motivates researchers to limit their studies to specific transient scenarios. For example, several authors consider pressure ramps of variable slope and study the influence of the pressure rise rate on the selected regime [26, 27] or the transient duration [20]. In this article, we study rapid variations in control parameters through stochastic initial conditions, in cases of multistability between an equilibrium and a periodic regime. We are interested in situations where the musician moves quickly from one quasi-static configuration to another, as is the case during an attack [21, 28], a break or a change of note [22, 29, 30]. Quasi-statistical analysis is not valid during this transition and the new quasi-static configuration is studied under unknown initial conditions. With this in mind, we study the statistical influence of initial conditions on the selected regime and on the duration of the transient. The probability of obtaining each regime is estimated with an already existing method called basin stability [31], and an original approach is proposed to determine the probability of obtaining each transient duration. Finally, the distributions of initial conditions considered for these statistical methods are discussed. In particular, initial conditions generated by specific transient control scenarios are studied.

The remainder of the document is organized as follows. The system chosen to introduce the methods is given in Section 2. Section 3.1 focuses on the basin stability metric and its use for musical instruments. The transient duration is investigated in Section 3.2 and the influence of the distribution of initial conditions is explored in Section 4. To highlight the interest of the methods on more sophisticated and high dimensional systems, an application to a physical model of trumpet is presented in Section 5. Different methods and results are discussed in Section 6. Perspectives and conclusions are drawn in Section 7.

2 Minimal multistable system

Most physical models of self-sustained musical instruments have no exact analytical solutions for transient or steady-state regimes. Therefore, numerical methods are often used to study them, such as finite differences [32] or

harmonic balance method [33]. A number of authors have proposed less detailed models with exact analytical solutions and only few state variables. These simplified models help to investigate the mechanisms behind self-oscillations [34]. In order to compare our statistical approach with exact analytical results, we have chosen to illustrate our methods on such a system. In this article, we focus on a Van der Pol oscillator with fifth-order nonlinearity, as described in [35]. This oscillator is characterized by a region of multistability, where both an equilibrium and a periodic solution are stable. This feature can also be observed on several musical instruments, such as saxophones [27] or brass instruments [5]. Its phase space is of dimension two and can therefore be displayed simply, enabling more detailed dynamic analysis. A technical publication [36] presents the musical interest of this system and provides a demonstrator solving it in real time (<https://zenodo.org/records/8413627>). Note that even though the global behavior of musical instruments is varied and rich, the system studied here can be obtained by change of variables and polynomial expansions from any system presenting this type of multistable behavior. It is only used to illustrate the interest of a statistical approach to predict the behavior of a multistable system under transient excitations.

The motion of the considered oscillator is given by the following equation:

$$\ddot{x} + [-\mu + \sigma(x^2 + \dot{x}^2) + \nu(x^2 + \dot{x}^2)^2]\dot{x} + x = 0. \quad (1)$$

We impose $\sigma = -1.5$ and $\nu = 0.1$ in order to obtain a multistable saxophone-like or brass-like behavior. The parameter μ is the control parameter of this simple “musical instrument” and its effect is analogous to the blowing pressure for wind instruments [36]. A harmonic balance method with only one harmonic gives the amplitude X of solutions of the form:

$$x = X \cos(t + \varphi). \quad (2)$$

There are up to three solutions, depending on the value of μ :

$$\begin{cases} X_{Eq} = 0, \\ X_{2\pi+} = \sqrt{\frac{-\sigma + \sqrt{\sigma^2 + 4\mu\nu}}{2\nu}} & \text{if } \mu \geq \mu_{SN}, \\ X_{2\pi-} = \sqrt{\frac{-\sigma - \sqrt{\sigma^2 + 4\mu\nu}}{2\nu}} & \text{if } \mu_{SN} \geq \mu \geq \mu_H, \end{cases} \quad (3)$$

with $\mu_H = 0$ and $\mu_{SN} = -\frac{\sigma^2}{4\nu}$. These solutions consist of an equilibrium (X_{Eq}) and two 2π -periodic solutions ($X_{2\pi+}$ and $X_{2\pi-}$), which are represented on a bifurcation diagram in Figure 1. This oscillator shows an inverse Hopf bifurcation at $\mu = \mu_H$ and a saddle-node bifurcation at $\mu = \mu_{SN}$. Between these two bifurcations, the system is multistable: both the equilibrium X_{Eq} and the largest periodic solution $X_{2\pi+}$ are stable. Saxophones [27] and brass instruments [5] are likely to present this bifurcation sequence and therefore this multistability behavior.

A traditional bifurcation diagram only depicts the steady state solutions. The influence of initial conditions on the transient and the steady-state behavior is concealed.

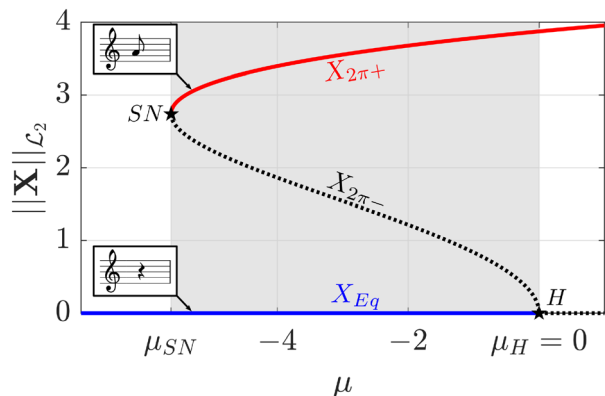


Figure 1. Bifurcation diagram of a fifth order Van der Pol oscillator equation (1) with respect to the control parameter μ , with $\sigma = -1.5$ and $\nu = 0.1$. Stable solutions are represented with continuous lines, unstable solutions in broken lines and bifurcations are indicated with star markers. The region of multistability is shaded in grey.

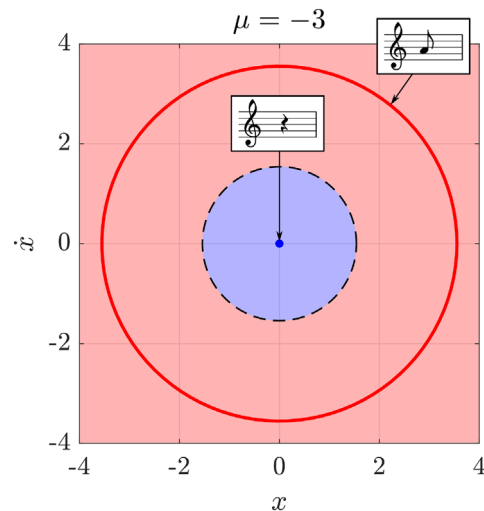


Figure 3. Basins of attraction of the fifth order Van der Pol oscillator ($\mu = -3$). Initial conditions taken in the red shaded area give rise to the periodic solution whereas initial conditions taken in the blue shaded area give rise to the equilibrium solution.

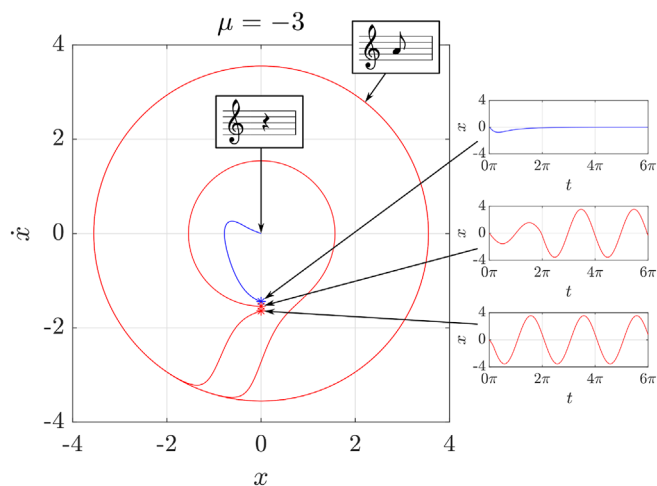


Figure 2. Illustration of the sensitivity to the initial conditions, for the Van der Pol oscillator, regarding the steady state regime and the transient duration. On the left side, the phase plane of the system for $\mu = -3$, with trajectories coming from three close initial states (indicated with star markers). On the right side, the evolution of the position x with respect to time (dimensionless).

1 This influence can be seen on a phase plane for a given value
 2 of the control parameters. In Figure 2, we show the phase
 3 plane of the fifth order Van der Pol oscillator for $\mu = -3$,
 4 which is a situation of multistability. For the remainder
 5 of the paper, we use this value each time we need to choose
 6 a specific μ for illustration. The equation of motion equation
 7 (1) is numerically integrated with the function ode45 of
 8 Matlab [37], for three initial states very close to one
 9 another. In that case, the slight change in initial conditions
 10 leads the system either to the equilibrium (in blue) or to the
 11 stable limit cycle (in red). The two oscillating trajectories
 12 have different transient durations: one is almost instantaneous
 13 while the other lasts approximately one period.

In short, Figures 1 and 2 illustrate that the steady state and the transient duration of this minimal self-sustained musical instrument are sensitive to the initial conditions and to the control parameter value around a bifurcation. This sensitivity is merely a mark of non linearity and is shared by most non linear dynamical systems. In the Sections 3.1 and 3.2, we present two statistical approaches to predict the selected regime and the transient duration for such a system.

3 Methods

3.1 Basin stability

Some self-sustained musical instruments are multi-stable. In such a case, once their control parameters are settled, their steady state depends exclusively on their initial state. The subset of initial conditions leading to a specific attractor is called its basin of attraction [38, 39]. In Figure 3, we depict the basins of attraction of the fifth order Van der Pol oscillator, for $\mu = -3$. The basin of the equilibrium is shaded in blue and the basin of the periodic solution is shaded in red. In that case, the two basins are separated by the unstable limit cycle of amplitude $X_{2\pi-}$, plotted in broken line and given in equations (1) and (3). In the general case, however, the geometry of a basin of attraction can be more complex and its boundaries difficult to find. We discuss this problem in Section 6. Moreover, in the scope of this article, we consider that the initial conditions resulting from a quick change in the control parameters are unknown. They are randomly taken within a subset of the initial state space. Since the initial state is unknown, the precise geometry of the basins of attraction does not suffice to predict its playing regime.

To take into account the uncertainty of the initial state, we propose to use the notion of *basin stability*, a probabilistic metric introduced by [31]. The principle is to evaluate the size of the basins of attraction with respect to the total size of the considered space of initial states. The result gives the probability to reach each attractor, considering a random initial state. Formally, considering a subset of interest of the space of initial conditions \mathcal{Q} , an attractor A , its basin of attraction B and a probability density function ρ , the basin stability $\mathcal{S}_B(A)$ is defined as follows:

$$\mathcal{S}_B(A) = \int_{\mathcal{Q}} \mathbf{I}_B(\mathbf{X}) \rho(\mathbf{X}) d\mathbf{X}, \quad (4)$$

where

$$\mathbf{I}_B(\mathbf{X}) = \begin{cases} 1, & \text{if } \mathbf{X} \in B, \\ 0, & \text{otherwise.} \end{cases} \quad (5)$$

The probability density function ρ can follow a specific distribution if the random choice of initial conditions is not uniform. This aspect is discussed in Sections 4 and 6. Due to the nature of ρ as a probability density function over \mathcal{Q} , the basin stability metric is always comprised between 0 and 1. $\mathcal{S}_B(A) = 0$ indicates that the basin of attraction of the solution is statistically never reached. $\mathcal{S}_B(A) = 1$ means that the basin of attraction of A occupies all of the region of interest \mathcal{Q} , and that A is reached by every trajectory. All the illustrations of Section 3 are realized with a uniform distribution. The volumic integral in the expression equation (4) of \mathcal{S}_B is rarely calculable exactly and we rather compute the corresponding discrete sum. In other words, we take N random samples in \mathcal{Q} and we evaluate the proportion of samples belonging to the studied basin of attraction. The basin stability estimation, which is noted $\hat{\mathcal{S}}_B$, then writes:

$$\hat{\mathcal{S}}_B(A) = M/N, \quad (6)$$

where M is the number of samples belonging to B , the basin of attraction of A . As pointed out in [31, 40, 41], this computation corresponds to N independent trials with probability of success \mathcal{S}_B . The resulting standard error due to sub-sampling writes:

$$\text{err}(\hat{\mathcal{S}}_B) = \sqrt{\frac{\mathcal{S}_B(1 - \mathcal{S}_B)}{N}}. \quad (7)$$

In practice, \mathcal{S}_B is unknown so it is replaced by its estimation $\hat{\mathcal{S}}_B$ in equation (7). This error only accounts for sub-sampling. It is interesting to notice that the error does not depend on the dimension of the state space. As a result, the basin stability is a metric suitable for low dimension problems as well as for high dimension ones. In general, for more complex systems, the basin boundaries are unknown and the classification method would consist in time integrating the system and observing toward which attractor it would converge. Such strategy is illustrated in Figure 4. However, for this minimal multistable system, the basin boundary is analytically known: the boundary is the unstable periodic solution whose \mathcal{L}_2 -norm $X_{2\pi-}$ is given

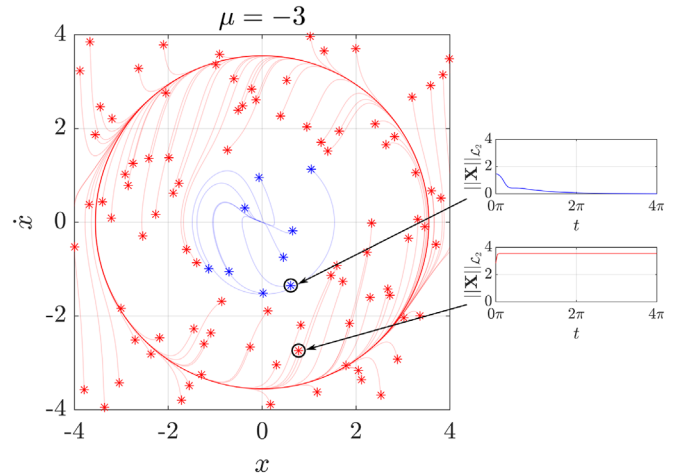


Figure 4. Illustration of the classification method in the general case. The plotted trajectories are obtained with time integrations starting from the stars as initial conditions. Red trajectories are inside the basin of attraction of the stable periodic solution $X_{2\pi+}$ whereas the blue ones belong to the basin of the equilibrium X_{E_q} .

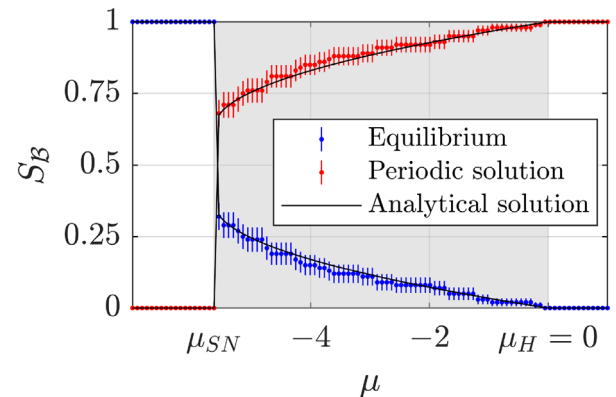


Figure 5. Basin stability of the two stable solutions computed from 100 samples. In red: basin stability of the periodic solution. In blue: basin stability of the equilibrium. Error bars correspond to the standard error of the size estimation of the Monte-Carlo method due to sub-sampling equation (7). In black: basin stability computed with the analytic expression of the basin boundary (circle of known diameter $X_{2\pi-}$ given in (3)). The region of multistability is shaded in grey.

in equation (3). As a result, it is much faster to classify the samples with this analytical expression rather than with time integrations.

Figure 5 gives the basin stability of the Van der Pol oscillator. To compute it, we arbitrarily choose a subset of the phase space \mathcal{Q} which includes all the attractors and which is independent of μ . For $\mu \in [-7, 1]$ as in Figure 1, the subset $\mathcal{Q} = ([-4, 4] \times [-4, 4])$ meets these conditions. To uniformly sample \mathcal{Q} , we use a Latin Hypercube Sampling of 100 samples. The basin stability of the equilibrium is plotted in blue and the one corresponding to the periodic solution in red. The error bars correspond to the

1 standard error given in equation (7). In addition, within the
 2 multistability region, i.e., for $\mu_{\text{SN}} \geq \mu \geq \mu_{\text{H}}$, the exact basin
 3 stabilities write:

$$\begin{cases} S_{\mathcal{B}}(X_{\text{Eq}}) = \frac{\pi X_{2\pi-}^2}{\text{area}(\mathcal{Q})}, \\ S_{\mathcal{B}}(X_{2\pi+}) = 1 - S_{\mathcal{B}}(X_{\text{Eq}}). \end{cases} \quad (8)$$

6 These exact solutions are represented with black lines. They
 7 mainly remain inside the error bars estimated with $\hat{S}_{\mathcal{B}}$ (i.e.,
 8 $S_{\mathcal{B}}$ replaced by $\hat{S}_{\mathcal{B}}$ in Eq. (7)). This validates the error esti-
 9 mation of the sample-based method given in equation (7).
 10 Outside the multistability area, the only stable solution
 11 has a basin stability equal to 1 whereas the other one has
 12 a basin stability equal to 0. Regarding this metric, non
 13 existing solutions and unstable solutions are identical and
 14 have a zero basin stability. Inside the multistability area,
 15 both solutions have a non zero basin stability. The stability
 16 of the periodic solution increases with μ whereas the stabil-
 17 ity of the equilibrium decreases. One can observe that $S_{\mathcal{B}}$
 18 is continuous at the Hopf bifurcation but discontinuous at the
 19 saddle-node bifurcation. Indeed, in the first case, the basin
 20 of attraction of the equilibrium shrinks progressively until it
 21 becomes a dot in the phase space for $\mu = \mu_{\text{H}}$. In the second
 22 case, the periodic solution suddenly disappears at μ_{SN} , even
 23 though its basin of attraction had previously occupied a
 24 large part of \mathcal{Q} . The value of $S_{\mathcal{B}}$ corresponds to the proba-
 25 bility to obtain the related solution, given a random initial
 26 state inside \mathcal{Q} . If a musician were to impose uniformly ran-
 27 dom initial conditions in $\mathcal{Q} = ([-4, 4] \times [-4, 4])$, Figure 5
 28 indicates that he/she would have at least a 60% chance of
 29 reaching the periodic regime in the steady state. However,
 30 the assumption of a musician peeking a random initial
 31 condition uniformly seems oversimplified. This topic is
 32 discussed in Sections 4 and 6.

33 Overall, the basin stability indicates which values of the
 34 parameters (here, the only parameter is μ) fosters one
 35 solution or another. It gives the probability to produce a specific
 36 regime, considering a subset \mathcal{Q} of the phase space and a
 37 probability density function ρ of \mathcal{Q} . The result depends
 38 greatly on the choice of \mathcal{Q} and ρ . The standard error of this
 39 metric depends on the number of samples and on the rela-
 40 tive size of the studied basin of attraction. It does not
 41 depend on the phase space dimension however and thus is
 42 very well adapted to high but finite dimensional systems.

45 3.2 Transient duration

46 In music, transient phenomena play a crucial role in
 47 sound and instrument discrimination [42–44]. Musicians
 48 may also have expectations concerning the characteristics
 49 of these transients, and in particular concerning their
 50 duration. For example, Guettler and Askenfelt [23] high-
 51 light the importance of the type and duration of violin
 52 attacks on their quality as perceived by professional string
 53 players. Several authors [21, 22, 25, 45] assume that musi-
 54 cians and instrument makers look for short transitions,
 55 whether for the onset or for sequences of linked notes.
 56 In this paper, we thus consider the reaction time of an

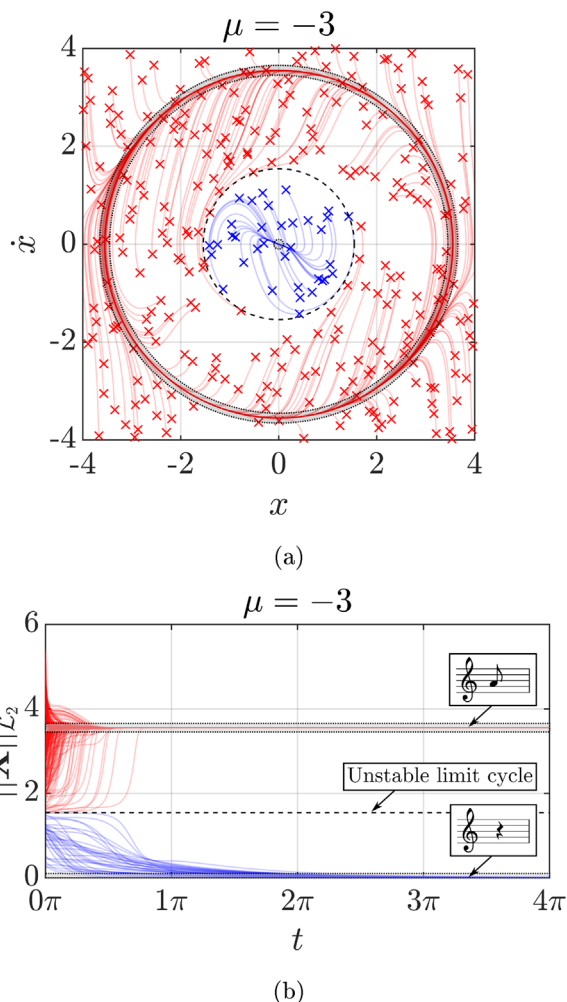


Figure 6. (a) Phase trajectories and (b) time evolution of the associated norm of the system’s state for 300 random initial conditions. Blue trajectories lead to the equilibrium and red trajectories lead to the periodic solution. The neighborhoods of the two stable solutions are shaded in grey. They are defined at a distance $\varepsilon = 0.1$ in \mathcal{L}_2 -norm from the stable solutions.

instrument – i.e., its tendency to produce short transients –
 as a playability criterion. In self-sustained instruments, the
 transient depends on the parameters of the system but also
 on the initial conditions, as can be seen on Figure 6. In this
 figure, the evolution of the fifth order Van der Pol oscillator
 has been computed for a large number of random initial
 states, all other things being equal. In Figure 6a, the trajec-
 tories are represented in the phase plane whereas in
 Figure 6b, the same trajectories are represented with respect
 to time. The transient part of a trajectory is defined between
 its initial state and the moment it reaches the neighborhood
 of an attractor. The transient duration is denoted τ here-
 after. The neighborhoods of the two attractors are shaded
 in grey and are defined at a distance ε in \mathcal{L}_2 -norm from
 the attractor. Although the size of these neighborhoods
 has an impact on the transient duration results, for now
 it is arbitrarily set to $\varepsilon = 0.1$. Figure 6b highlights the
 diversity of transient durations that can be obtained only

57
58
59
60
61
62
63
64
65
66
67
68
69
70
71
72
73
74

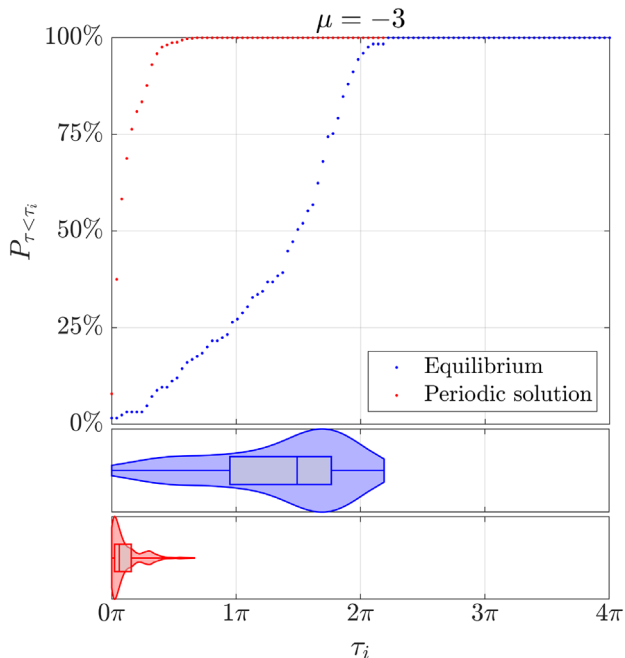


Figure 7. (Top) Cumulative probability function of the transient duration distribution. In ordinate, the proportion of trajectories with a transient duration below the value given in abscissa. (Bottom) Corresponding violin plots. The box plots indicate the extreme values, the median, the upper and lower quartiles whereas the curves around represent the probability density function of the transient duration distribution. A latin hypercube of 1000 samples is used and the transient durations are defined with $\varepsilon = 0.1$.

1 by picking different initial conditions. Some tendencies seem
 2 to appear. For instance, for this distribution of initial condi-
 3 tions, trajectories leading to the equilibrium are usually
 4 longer than those leading to the periodic solution.

5 These tendencies stand out when the distributions of
 6 the transient durations are represented graphically. Informa-
 7 tion on a distribution can be displayed as in Figure 7.
 8 The upper panel gives the cumulative distribution function,
 9 i.e., the proportion of trajectories with a transient duration
 10 shorter than the value τ_i represented in abscissa. The two
 11 lower panels depict the corresponding violin plots [46, 47],
 12 where the box plots give the extreme values (tips of the
 13 whiskers), the median and the two quartiles, and the shaded
 14 curves represent the probability density function of the distributions.
 15 To compute the latter, we used the kernel density estimator
 16 of Matlab (ksdensity). This statistic information is calculated
 17 for each attractor separately. As in Section 3.1, we use a Latin
 18 Hypercube Sampling to uniformly explore the space of initial
 19 states. With this sampling, we do not control the exact number
 20 of samples in each basin of attraction, but it can be estimated
 21 with the basin stability \mathcal{S}_B previously computed. As a result,
 22 for lowest values of \mathcal{S}_B , the statistical transient analysis
 23 relies on only few samples and may not be very representative.
 24 It should be remembered that such misrepresentations
 25 occur only on highly improbable regimes. If a specific

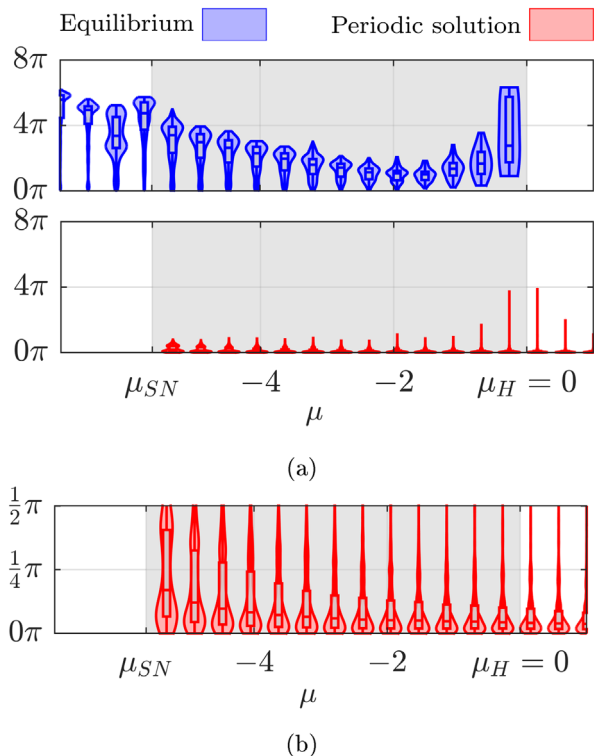


Figure 8. Violin plots of the transient duration with respect to the control parameter μ . In blue: equilibrium. In red: periodic solution. Number of samples: $N = 1000$. Panel (b) is a magnified version of the transients leading to the periodic solution. The region of multistability is shaded in grey.

case calls for in-depth study of these regimes, the region
 of interest \mathcal{Q} can be adapted, leaving the method otherwise
 unchanged. The cumulative distribution function lends
 itself well to interpretation in musical context, where one
 could define a longest acceptable transient duration. The
 probability of the transient being shorter than this upper
 limit can be read directly on the cumulative distribution
 function, under the hypothesis of random initial conditions
 following a uniform law.

We use the violin plot representation in Figure 8 to
 depict the evolution of the transient duration distribution
 with respect to the control parameter μ . Plotting the
 probability density function over the boxplot is particularly
 interesting when there are multiple maxima in the distribu-
 tion since multiple maxima are not visible on a box plot.
 For instance, some examples of bi-modal distributions can
 be observed around the saddle-node bifurcation (for
 $\mu \approx \mu_{SN}$).

Figure 8 shows that most transients leading to the
 periodic solution are very short compared with its period
 ($T = 2\pi$). Indeed, the violin plots are centered around
 low values of τ (a magnified view for $\mu = -3$ is visible
 in Fig. 9). However, the maximum transient durations are
 markedly larger than the median duration, up to 800 times
 longer for $\mu = -0.26$. This indicates that, for most values
 of μ , a few initial conditions have extremely long transients.

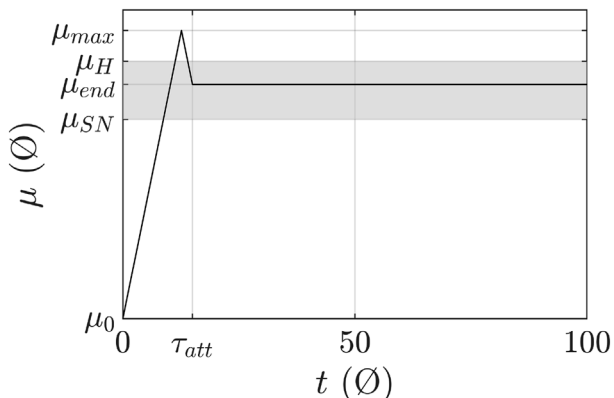


Figure 9. Control scenarios used to compute the transient-informed initial conditions. The multistability region is shaded in gray. μ_0 is the initial value of μ , μ_{\max} is the overshoot, μ_{end} is the final value of μ , at which the basin stability is computed, μ_H and μ_{SN} are the value of μ at the Hopf and at the saddle-node bifurcations and τ_{att} is the attack duration.

In fact, these particular initial states are very close to the unstable limit cycle. In that case, the trajectory follows the unstable limit cycle for some time while slowly diverging from it, which lengthens the transient duration. These rare and very long durations have particularly large values in the vicinity of the Hopf bifurcation. For the equilibrium, transient durations are longer and distributed more uniformly for all the values of μ . Outside the vicinity of the two bifurcations, the transient durations leading to both solutions statistically decrease as μ increases. This is coherent with the fact that $-\mu$ is the linear part of the damping. As μ increases, the system becomes less and less damped until μ eventually becomes positive and energy is added to the system. Near the saddle-node bifurcation, this trend does not apply. The equilibrium becomes the only stable solution but its transient duration globally increases around μ_{SN} . This is a usual phenomenon around a saddle-node bifurcation. It is interpreted by Strogatz in [38] as the remaining *ghost* of a nearby attractor that does not exist anymore. Around the Hopf bifurcation, the periodic solution becomes the only stable solution but its maximum transient duration significantly increases. However, apart from these very few long transients, Figure 8b shows that the overall trend does not change significantly for the periodic solution around the Hopf bifurcation. Considering initial conditions chosen from a uniform distribution, these long transients are highly improbable.

4 Influence of the distribution of initial conditions

In order to provide a more meaningful analysis in a context of musical performance, we consider another distribution for the initial conditions, informed by temporal evolutions of the control parameter. More precisely, we now consider initial conditions resulting from a transient

variation of the control parameter μ , just before it reaches a constant target value. Our goal is therefore to consider what we call hereafter a “transient-informed” distribution and to analyze how it affects the basin stability results. To obtain a transient-informed distribution, we compute the time evolution of the system under several transient variations of μ . These transient-informed distributions could also be used to compute the transient duration statistics, but we only focus on the basin stability here, since the results are more remarkable.

4.1 Control scenarios

Systems such as the fifth order Van der Pol oscillator presenting an inverse Hopf bifurcation followed by a saddle-node bifurcation produce a sound of non-zero amplitude when the control parameter exceeds the Hopf bifurcation (this is the case for the trumpet and the saxophone for certain sets of parameters). Nevertheless, it is possible to reduce the sound amplitude afterward by decreasing the control parameter under the Hopf bifurcation value, into the multistability region. To produce a low-volume sound at the onset, one can attempt to realize this gesture quickly by reducing the control parameter, and move the system into the multistable region before the limit cycle is attained. However, this strategy may fail if the system remains too close to the equilibrium during the transient. It would become trapped in the equilibrium’s basin of attraction when the parameter stops varying, which would result in no stable sound being produced. We consider piecewise linear control scenarios, as depicted in Figure 9. These scenarios are defined by four parameters: their initial value μ_0 , their maximal value μ_{\max} that corresponds to what can be called the overshoot value, their final value μ_{end} at which the basin stability is computed and their duration τ_{att} that corresponds to the “attack duration”. For simplicity, we choose the same slope (in absolute value) for the increasing and the decreasing phases (before and after the overshoot).

The order of magnitude of μ_0 is based on the bifurcation diagrams of the trumpet models presented in [5]. The objective is to give as much importance to the multistability as in these trumpet models. Therefore μ_0 is set to have a similar ratio between the size of the multistability region $[\mu_{SN}, \mu_H]$ and the size of the stability region of the equilibrium $[\mu_0, \mu_H]$ as in the models of [5]. μ_0 is then set to $\mu_0 = -25$. At the end of the attack, $\mu = \mu_{\text{end}}$ and the basin stability is computed for this value of μ . The overshoot μ_{\max} and the duration of the attack τ_{att} are the two remaining parameters of the control scenarios. In the following, we study the influence of a given overshoot μ_{\max} on the regime selection, while the attack duration τ_{att} remains free to take different values. We arbitrarily choose $\mu_{\max} \in [1, 10]$ and $\tau_{\text{att}} \in [1, 20]$ (dimensionless values). In [21], Ernout and Fabre measured pressure rise times going approximately from 5 to 150 ms, for all fingerings between C5 (1046.5 Hz) and C6 (2093 Hz). Therefore, by choosing $\tau_{\text{att}} \in [1, 20]$, we keep a ratio between the longest and the shortest attacks with the same order of magnitude as in [21].

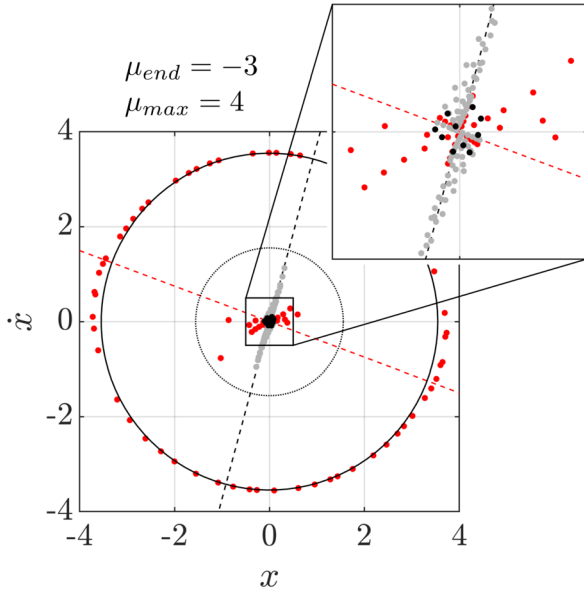


Figure 10. Example of a transient-informed distribution generated with 10 control scenarios of different durations. (•) Pre-initial Latin Hypercube of size $N_0 = 10$; (•) states of the system when $\mu = \mu_{\max}$; (•) transient-informed distribution at the end of the attack. The black dotted line is the fast eigendirection of the equilibrium at $\mu = \mu_{\max}$ and the red one is its slow eigendirection at $\mu = \mu_{\text{end}}$.

4.2 Distribution generation

To generate a transient-informed distribution of initial conditions for a specific μ_{end} , we apply 10 control scenarios with different durations ($\tau_{\text{att}} \in [1, 20]$) and with a unique value of μ_{\max} , to $N_0 = 10$ pre-initial conditions chosen close to the equilibrium (Latin Hypercube Sampling taken inside $x \in [-0.1, 0.1]$ and $\dot{x} \in [-0.1, 0.1]$). As a result, we obtain a transient-informed distribution of $N = 100$ initial conditions depicted in [Figure 10](#). Firstly, it can be observed that this distribution is far from being uniform; most transient-informed initial conditions are very close to either the equilibrium or the periodic solution. It is expected for such a system to leave an unstable equilibrium through its fast eigendirection (i.e., associated with the eigenvalue of highest modulus) and to converge towards a stable equilibrium through its slow eigendirection (i.e., associated with the eigenvalue of smallest modulus). Such behavior is explained by Strogatz in example 5.2.3, p.133 of [\[38\]](#). Precisely, around the equilibrium in [Figure 10](#), the states of the system at $\mu = \mu_{\text{end}}$ are gathered along a specific direction whereas the states of the system at $\mu = \mu_{\max}$ are regrouping along another direction. In addition, we plot on the same figure the fast eigendirection of the equilibrium at $\mu = \mu_{\max}$ and its slow eigendirection at $\mu = \mu_{\text{end}}$. At the overshoot, the system clearly leaves the equilibrium through its fast eigendirection. At the end of the attack, some of the trajectories converge toward the equilibrium. If the simulation was performed over a longer duration, they would eventually gather along the slow eigendirection of the equilibrium.

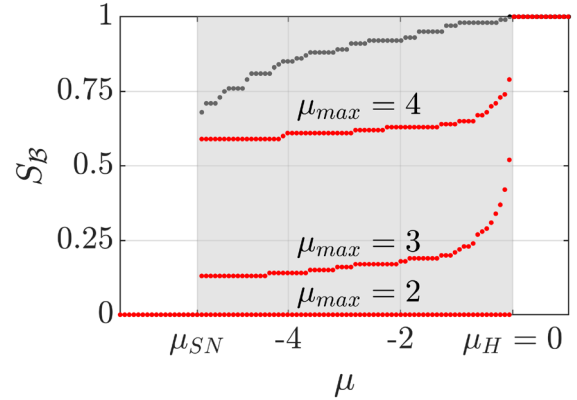


Figure 11. Basin stability of the periodic solution computed with different distributions. The red curves are computed with transient-informed distributions of initial conditions, each curve corresponding to a specific overshoot $\mu = \mu_{\max}$. The black curve is computed with a uniform distribution (it is the same as in [Fig. 5](#) without the error bars).

4.3 Basin stability with transient-informed distribution

The basin stability is then computed using these transient-informed distributions. The results are shown in [Figure 11](#) for three different overshoot values. For the sake of readability, only the basin stability of the periodic solution is represented (we recall that the basin stability of the equilibrium is the complementary to one).

The result computed with the uniform distribution is represented in black. Firstly, this [Figure 11](#) highlights that the basin stability depends greatly on the considered distribution, even though some features are preserved: $\mathcal{S}_B(\mu)$ is discontinuous at $\mu = \mu_{\text{SN}}$, continuous at $\mu = \mu_{\text{H}}$ and monotonously increasing for the cases where $\mu_{\max} = 3$ and 4. In the case where $\mu_{\max} = 2$, the overshoot scenario does not suffice to leave the basin of the equilibrium and no oscillations are observed in the multistable region. Secondly, for the situation considered, this [Figure 11](#) shows that the large-overshoot attacks are more likely to make the system end up on the periodic solution. Moreover, the basin stability increases faster when μ_{end} gets closer to μ_{H} . In terms of playability, a slowly varying \mathcal{S}_B can be interpreted as a region where the difficulty to produce a sound does not depend much on the final value of the control parameter. For the situation under study, this means that for a given value of μ_{\max} , all the attacks with μ_{end} in this region of slow varying \mathcal{S}_B have almost the same probability to converge towards the periodic solution. As a result, if we ignore the difficulty for a musician to maintain $\mu > \mu_{\text{SN}}$, there is no additional difficulty to reducing the sound amplitude to its minimal value.

5 Application to a trumpet model

In order to evaluate the interest of the methods introduced in previous sections to a more advanced and high

31
3233
34
35
36
37
3839
40
41
42
43
44
45
46
47
48
49
50
51
52
53
54
55
56
57
58
59
60
61

62

63
64

1 dimensional model of musical instrument, the analysis of
 2 basin stability and transient durations is applied in this
 3 section to a physical model of B₃ trumpet.

4 5.1 Presentation of the model

5 The model used is identical to the one considered in [5].
 6 It is detailed in Appendix A. The lips are represented by a
 7 one-degree-of-freedom oscillator. The air column inside the
 8 body of the instrument, also known as the resonator, is
 9 modeled by a modal truncation of its input impedance.
 10 These two elements are coupled by a nonlinear function
 11 that models the air jet through the lip channel. In this arti-
 12 cle, we consider an 11-mode truncation of the resonator and
 13 fix the resonance frequency of the lips around the second
 14 impedance peak ($f_L = 200$ Hz and $f_2 = 232.7$ Hz). This peak
 15 corresponds to the lowest note of the instrument, in
 16 “normal” playing conditions (the first peak being associated
 17 with the “pedal note”). The variables of this model are the
 18 position and velocity of the lip as well as the real and
 19 imaginary parts of the 11 modal pressures. This results in
 20 a system of dimensionality 24. The parameter values used
 21 in this article are given in Appendix A.

22 5.2 Bifurcation diagram

23 Unlike the fifth-order Van der Pol oscillator, this
 24 trumpet model has no analytical solutions. To determine
 25 its solutions, numerical continuation can be used. Here,
 26 we use the Manlab software [33]. The bifurcation diagram
 27 of the model is shown in Figure B1. The amplitude of the
 28 mouthpiece pressure p and the frequency of the sound pro-
 29 duced f_{play} are plotted with respect to the blowing pressure
 30 p_0 . In this zone, the system exhibits an inverse Hopf bifur-
 31 cation followed by a saddle-node bifurcation, like the Van
 32 der Pol oscillator presented in previous sections. The
 33 periodic regime is associated with the second mode of the
 34 resonator, represented on the bottom panel of Figure B1
 35 by a horizontal dotted line.

36 5.3 Basin stability and transient durations computed 37 with bSTAB

38 To calculate the system’s basin stability and transient
 39 durations, we use the bSTAB toolbox [48]. For our applica-
 40 tion, we have made a number of modifications to this tool-
 41 box, which are detailed in Appendix B. These modifications
 42 rely on convergence criteria in order to identify when the
 43 system has reached steady state. The numerical integration
 44 lasts until these criteria are met, rather than for an arbi-
 45 trary time which would be identical for all trajectories.
 46 These modifications allow us both to reduce the duration
 47 of the time integrations required to compute basin stability,
 48 and to calculate the duration of transients (which is not
 49 provided in the original toolbox). These criteria must be
 50 defined carefully, in order to avoid samples missclassifica-
 51 tion, leading to errors in the estimation of basin stability
 52 and transient durations.

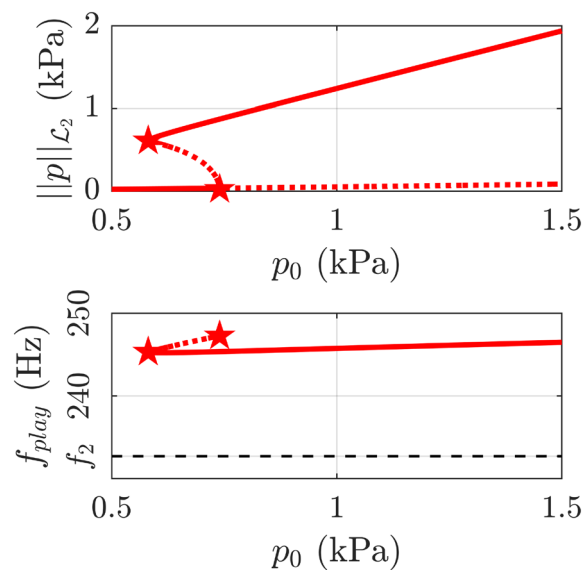


Figure 12. Bifurcation diagram of the 11-mode trumpet model, calculated with Manlab. Top pane: amplitude of the oscillations $\|p\|_{\mathcal{L}_2}$ versus blowing pressure p_0 . Bottom pane: fundamental frequency of the oscillations f_{play} versus blowing pressure p_0 . Stable solutions are shown as solid lines, unstable solutions as dotted lines. Bifurcations are represented by stars.

53 5.3.1 Initial conditions from a uniform distribution

54 As for the Van der Pol oscillator, we first consider a
 55 uniform random distribution of initial conditions \mathcal{Q}_u
 56 selected inside a hyper-rectangle. This hyper-rectangle is
 57 chosen large enough to contain all the solutions, whatever
 58 the value of p_0 . Its bounds are set as the extrema of the
 59 stable periodic solution at $p_0 = 0.8$ kPa, rounded up to
 60 the nearest integer value.

61 The basin stability calculated with \mathcal{Q}_u for $N = 300$
 62 samples is given in Figure 13a, the transient duration distri-
 63 butions are given in Figure 13b and a zoomed-in view is
 64 given in Figure 13c. The basin stability shares some features
 65 with the Van der Pol oscillator. Indeed, it is discontinuous
 66 at the saddle-node bifurcation and remains continuous at
 67 the Hopf bifurcation. The observations and comments
 68 made about this feature on the simple Van der Pol oscilla-
 69 tor translate directly to this more complicated system. In
 70 addition, \mathcal{S}_B is monotonous. However, unlike the Van der
 71 Pol oscillator, for dynamical systems of dimensionality
 72 three or more, the basins’ boundaries are different than
 73 the unstable periodic solutions. These objects even have
 74 different dimensionalities (the basins’ boundaries are hyper-
 75 surfaces and the limit cycles are hyperlines). Consequently,
 76 the basin stability of the equilibrium cannot be inferred
 77 from a size estimate of the unstable periodic solution and
 78 the sampling approach is then required.

79 Concerning transient durations, the Hopf bifurcation
 80 induces a few long transients in its vicinity, leading both
 81 to the equilibrium and to the periodic solution. This is prob-
 82 ably related to the increasing timescale of the slowest
 83 eigendirection whose stability is reversed at the Hopf

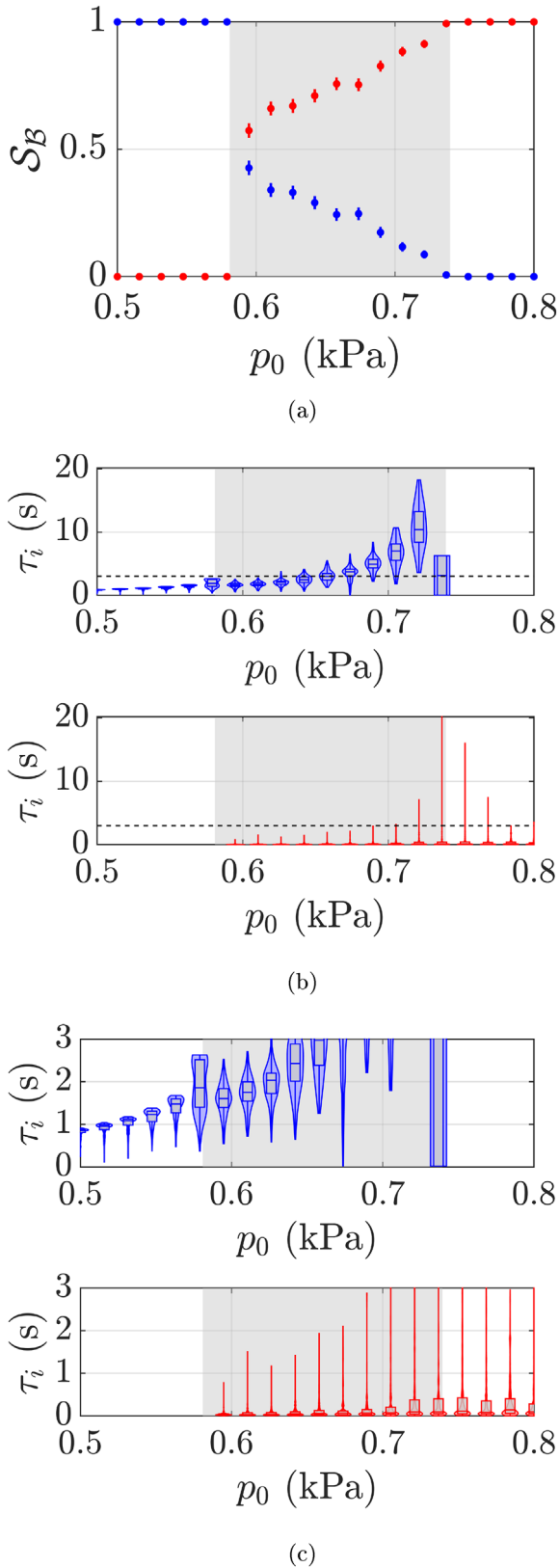


Figure 13. Basin stability (a) and transient duration distributions (b) of the trumpet model calculated with a uniform \mathcal{Q}_u distribution of $N = 300$ initial conditions. The dotted lines in (b) indicate the limit of the scale used for the zoomed view in (c). Error bars are given by the equation (7).

bifurcation. Eventually, the timescale of this eigendirection goes to the infinity at the Hopf bifurcation. The ghost effect around the saddle-node bifurcation, where the periodic solutions do not exist yet, is also visible but less than for the Van der Pol oscillator. This may be due to the fact that in a phase space of dimensionality two, for a value of the control parameter slightly below the value of the saddle-node, the trajectories initiated far away from the equilibrium necessarily have to enter the region of influence of this ghost limit cycle. On the contrary, in a phase space of higher dimensionality, these trajectories can pass away from this region. Moreover, the median and the interquartile range of both solutions increase around the Hopf bifurcation (even though it is hardly noticeable for the periodic solution with that scale).

Finally, this trumpet model sometimes exhibits transients of more than several seconds, which is extremely long compared to usual musical timescales. Beyond a certain duration, these asymptotic regimes can be considered unplayable or at least difficult to play. However, the regime that is heard during one of these extremely long transients can be treated as a playable regime by the musician, even if it is unstable. In this respect, one could see a percussion instrument as a dynamic system with only one asymptotic solution, the equilibrium, but whose transients are long enough to be used to make music. We could then consider a “transient” category for samples with a transient duration exceeding a certain “musical duration”, rather than classifying them according to their asymptotic solution.

5.3.2 Initial conditions from a distribution based on archetypal time variations of p_0

In the following, we study the influence of attack transients on basin stability. We apply the same method as in Section 4 to generate distributions \mathcal{Q}_b based on transient evolutions of p_0 . Again, we consider pressure rises with overshoot (see Fig. 9), in the manner of a strong tonguing attack or a sforzando, as can be found in [49]. The configuration and the parameters chosen here differ from [49]. Consequently, we consider slightly different control transients than those measured in that article, so that $p_{0,\max} \in [1, 10]$ kPa and $\tau_{\text{att}} \in [10, 500]$ ms. Ten attack transients are applied to each sample of a uniform distribution of $N_0 = 100$ pre-initial conditions. This leads to a final distribution of $N = 1000$ initial conditions. Each variable of the pre-initial distribution is selected in ranges 0.3 times smaller than in Section 5.3.1. These ranges are chosen arbitrarily and have a significant influence on the results.

In Figure 14a, we present the influence of the attack duration τ_{att} on the behavior of the system. Each curve has a fixed value of τ_{att} and 10 different values of $p_{0,\max} \in [1, 10]$ kPa. It is striking to see that the basin stability does not evolve monotonously with τ_{att} . Indeed, one would expect that the longer the system stays in the region of monostability of the periodic solution, the higher the chances it has to end up in its basin of attraction.

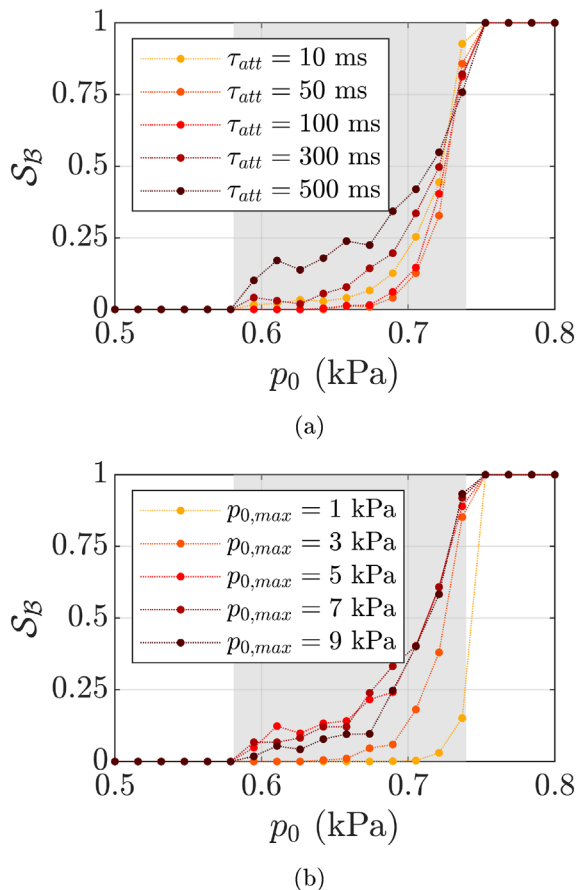


Figure 14. Basin stability of the trumpet model calculated with distributions \mathcal{Q}_{ib} of $N = 1000$ initial conditions based on attack transients (10 scenarios applied to each of the $N_0 = 100$ pre-initial conditions). (a) Each curve corresponds to a specific attack duration τ_{att} . (b) Each curve corresponds to a specific overshoot value $p_{0,max}$. Only the basin stability of the periodic regime is shown.

1 However, when τ_{att} increases from 10 to 50 ms, S_B
 2 decreases. S_B does not evolve much for $\tau_{att} \in [50, 100]$
 3 ms, and it then increases, as expected, for $\tau_{att} > 100$ ms.
 4 These observations can be analyzed by considering recent
 5 results concerning dynamical bifurcations [50]: how close
 6 the system has come to the equilibrium when the Hopf
 7 bifurcation is crossed is crucial to predict the dynamics
 8 above the bifurcation. This closeness is the result of the time
 9 spent by the system below the bifurcation but also of the
 10 number of significant digits used in the simulation (numerical
 11 noise is therefore inevitable). This makes direct inter-
 12 pretation not straightforward. In Figure 14b, we study
 13 instead the influence of the overshoot amplitude $p_{0,max}$ for
 14 various attack durations $\tau_{att} \in [10, 500]$ ms. In that case,
 15 S_B increases with the overshoot value, until it reaches its
 16 maximal value for $p_{0,max} \in [5, 7]$ kPa. Hence, it seems that
 17 there are optimal values of transient control parameters to
 18 maximize S_B . Further study would be needed to under-
 19 stand the dynamical reasons leading to this non trivial
 20 behavior.

6 Discussion

6.1 Computational cost

The methods presented in this paper allow to compute the basin stability and the transient duration distributions of a system. These metrics describe the global, statistical behavior of a system and could be very useful to study musical instruments, notably their playability. However, in order to take into account all the potential behaviors of a system, their computation can be costly. As a result, the computation cost limits the possible applications of these methods, for parametric studies for example.

Initially, [31] proposed to use Monte-Carlo techniques to numerically estimate the basin stability. Some limitations of these techniques have been drawn [40] when applied on strange basins of attraction (e.g., fractal and riddled/intermingled). However, such basins remain to be exhibited on self-sustained musical instruments. Some authors also proposed enrichment to the metric, to take into account uncertainties and variations of the parameters [51, 52]. Additionally, improvements on classical Monte Carlo approaches, notably using machine learning tools, show promise to accelerate basin stability computation. This could be interesting for more complex musical instrument models. For example, [41] proposed a method based on support vector machines. The idea is to find the basins' boundaries with a limited number of samples. Work still needs to be done to determine which method should be used depending on the situation and on the classification cost of a single sample. Indeed, if the classification of each sample is fast, it may be slower to find basins' boundaries rather than to apply a simple Monte-Carlo size estimation. For instance, it is the case for the Van der Pol oscillator presented in this article.

If the transient duration statistics and the basin stability are both studied, the two metrics can be computed simultaneously, using the same time integrations (as in Sect. 5). The cost needed to compute the basin stability with Monte-Carlo methods only depends on the size of the basin as indicated by the absolute standard error given by equation (7). For systems with higher dimensions, that cost could increase if the classification cost does. Moreover, the relative standard error, which writes $\text{err}_{rel}(\hat{S}_B) = \sqrt{\frac{1/S_B - 1}{N}}$, increases as S_B decreases. Higher dimension systems may have more stable solutions which lead to smaller basin stability values. More samples would thus be needed to keep the relative standard error low. This standard error formula stands for independent trials with only two outcomes – the sample is either inside or outside the studied basin of attraction. The calculation of the transient duration distributions does not enter into this category since the outcome is a continuous random variable: a transient duration. With a sparse sampling, some transient behaviors that appear for specific initial conditions might be missed. Consequently, it could be interesting to estimate the convergence of the probability density functions in order to chose an adequate number of samples.

The statistical methods presented here can be applied applied at low computational cost on the fifth order

21

22

23

24

25

26

27

28

29

30

31

32

33

34

35

36

37

38

39

40

41

42

43

44

45

46

47

48

49

50

51

52

53

54

55

56

57

58

59

60

61

62

63

64

65

66

67

68

69

70

71

72

73

74

75

76

77

78

1 Van der Pol oscillator, because the two attractors and the
 2 boundary of the basins of attraction are analytically known
 3 and characterized by their \mathcal{L}_2 -norm. On more complex
 4 systems, the attractors and basins' boundaries usually do
 5 not have analytic expressions. The main difficulty encoun-
 6 tered in carrying out the statistical analysis of the trumpet
 7 model presented in Section 5 was to define adequate classi-
 8 fication and stopping criteria. Indeed, non-linear systems
 9 sometimes evolve with very varied dynamics, making it dif-
 10 ficult to distinguish between a steady state and a transient
 11 regime with slow dynamics. This kind of behavior leads to
 12 significant differences in transient duration between differ-
 13 ent initial conditions, especially at a bifurcation, where
 14 one eigendirection becomes infinitely slow. These discrepan-
 15 cies in transient durations are particularly visible in
 16 Figure 13b, around the Hopf bifurcation. In this regard,
 17 the Manlab solutions were very helpful to define efficient
 18 classification and convergence criteria (see Appendix B).
 19 For systems with a wide range of transient durations, we
 20 would strongly recommend to set a convergence criteria
 21 rather than to use a fixed integration time, as this is the
 22 case in the version of bSTAB currently online. This would
 23 improve performances and limit missclassification.

24 6.2 Initial conditions and musical gestures

25 In Section 3, the presented statistical approach is based
 26 on a uniform distribution of initial conditions. This is a gen-
 27 eral distribution and it allows different instrument configu-
 28 rations to be compared. However, the resulting probabilities
 29 probably fail to translate the musician's playing experience.
 30 As a first attempt to tackle this issue, we study in Section 4
 31 initial conditions resulting from an archetypal control
 32 gesture. This approach highlights the importance of the
 33 considered distribution of initial conditions and it can be
 34 interpreted in musical terms more directly than random
 35 initial conditions. We would like to draw the reader's atten-
 36 tion to the fact that the results obtained with this transient-
 37 based approach not only depend on the transient control
 38 parameters, but also on the choice of the pre-initial condi-
 39 tions. Overall, applicative studies on playability would
 40 greatly benefit from a preliminary description of the control
 41 scenarios and, where relevant, initial conditions distribu-
 42 tions. In that perspective, it could be of great interest to
 43 measure transient blowing scenarios provided by humans
 44 (musicians and non-musicians) in an experimental study.
 45 Moreover, as illustrated by Figure 10, dynamical systems
 46 are more likely to cross specific regions of their phase space
 47 during transients. Choosing distributions of initial condi-
 48 tions based on the slow and fast eigendirections (depending
 49 on the solutions that exist during the transient) could also
 50 be an interesting idea.

51 In this paper, we focus on initial conditions induced by
 52 the fast evolution of one control parameter. However, musi-
 53 cians may also impact the initial conditions by acting
 54 directly on a state variable. One example among many
 55 others is the use of the tongue in reed instruments to impose
 56 initial reed positions and velocities. Measurements of ton-
 57 gue-induced reed positions in a clarinet are presented in

[53] for example. To improve the statistical approaches,
 these initial conditions should also be taken into account.

6.3 Stability, transient duration and playability

61 Other studies were interested in predicting the transient
 62 duration of a self-sustained musical instrument [24, 25].
 63 A common approach is to linearize the system around an
 64 unstable equilibrium and to consider the exponential
 65 growth of a perturbation. This exponential growth depends
 66 on the positive real part of the eigenvalues of the matrix of
 67 derivatives (i.e., the jacobian matrix). This method is better
 68 adapted for studying initial conditions close to an equilib-
 69 rium solution. The Floquet theory might be used in the
 70 same way for initial conditions next to a periodic solution,
 71 although it has yet to be applied in that manner to a musi-
 72 cal instrument model (for more details on the Floquet the-
 73 ory, refer to [54, 55]). In this article, we consider initial
 74 conditions not necessarily close to any solution. Hence,
 75 these linear analyses might not be valid for every sample.
 76 On more complex systems with several competing multi-
 77 stable solutions, its local nature prevents it from giving a
 78 complete analysis of the transients. However, the system-
 79 atic and fast nature of linear analysis makes it a good
 80 candidate to bolster certain sections of a complete statisti-
 81 cal study.

82 Finally, the statistical study of the trumpet model pre-
 83 sented in Section 5 highlights several interests of the meth-
 84 ods. The long transients observed in Figure 13 raise the
 85 question of the playability of a regime as a function of its
 86 transient duration. In a standard musical context, we argue
 87 that a regime that takes several seconds to establish cannot
 88 really be considered playable. Therefore, certain stable
 89 regimes could actually be unplayable due to transient
 90 behaviors, which shows the relevance of nuancing the
 91 notion of stability using transients when studying playabil-
 92 ity. The transient-based analysis of Section 5.3.2 also indi-
 93 cates that the transient control parameters of a musical
 94 gesture may have nontrivial optimal values. Future works
 95 could analyze these types of transient control scenarios into
 96 more details, relying on the statistical approaches as play-
 97 ability guidelines.

7 Conclusion and perspectives

99 In this article, we present a sample-based approach that
 100 can be used to enrich a bifurcation diagram. In this study
 101 we use it to investigate two playability issues: the prediction
 102 of the steady state in multistable situations and the predic-
 103 tion of the transient duration. The method used for the first
 104 issue is called the basin stability [31], whereas the method
 105 proposed for describing the responsiveness of a dynamical
 106 system is new, to the authors' knowledge. These two
 107 methods rely on distributions of initial conditions that
 108 represent the transient action of a musician. The results
 109 strongly depend on this choice of distribution and we
 110 proposed a method based on time integration to generate
 111 transient-informed distributions.

The methods are then applied to a physical model of trumpet with the aim to evaluate their interest in a more practical case. The transient-based basin stability of this model present non trivial tendencies regarding some transient control parameters. Moreover, very long transients are highlighted, which raises the question of the playability of such asymptotic regime. Overall, these statistical methods show interest for the analysis of musical instruments, but they can also be extended to a large variety of systems.

Future works will focus on two aspects. First, these methods will be applied on musical instrument models in configurations showing multiple oscillating regimes and rich transients. Then, measurements on musicians will be conducted to evaluate the initial conditions that they induce, depending on the desired musical effect.

16 Q3 Data availability statement

17 No new data were created or analyzed in this study.

18 References

- 19 1. T. Idogawa, M. Shimizu, M. Iwaki: Acoustical behaviors of
20 Q5 an oboe and a soprano saxophone artificially blown. Some
21 problems on the theory of dynamical systems in applied
22 science, 1992, pp. 71–93.
- 23 2. T. Idogawa, T. Kobata, K. Komuro, M. Iwaki: Nonlinear
24 vibrations in the air column of a clarinet artificially blown.
25 Journal of the Acoustical Society of America 93, 1 (1993)
26 540–551.
- 27 3. K.Y. Takahashi, H.A. Kodama, A. Nakajima, T.A. Tachi-
28 bana: Numerical study on multi-stable oscillations of wood-
29 wind single-reed instruments. Acta Acustica united with
30 Acustica 95, 6 (2009) 1123–1139.
- 31 4. J. Bocanegra, D. Borelli: Review of acoustic hysteresis in
32 flute-like instruments, in: Proceedings of 26th International
33 Congress on Sound and Vibration, Canada, Montreal, 7–11
34 July, 2019.
- 35 5. V. Fréour, L. Guillot, H. Masuda, E. Tominaga, Y. Tohgi, C.
36 Vergez, B. Cochelin: Numerical continuation of a physical
37 model of brass instruments: Application to trumpet compar-
38 isons. Journal of the Acoustical Society of America 148, 2
39 (2020) 748–758.
- 40 6. J.J. Jiang, Y. Zhang: Chaotic vibration induced by turbulent
41 noise in a two-mass model of vocal folds. Journal of the
42 Acoustical Society of America 112, 5 (2002) 2127–2133.
- 43 7. R.T. Schumacher, J. Woodhouse: The transient behaviour of
44 models of bowed-string motion. Chaos: An Interdisciplinary
45 Journal of Nonlinear Science 5, 3 (1995) 509–523.
- 46 8. T.A. Wilson, G.S. Beavers: Operating modes of the clarinet.
47 Journal of the Acoustical Society of America 56, 2 (1974)
48 653–658.
- 49 9. N.H. Fletcher: Nonlinear interactions in organ flue pipes.
50 Journal of the Acoustical Society of America 56, 2 (1974)
51 645–652.
- 52 10. B. Lawergren: On the motion of bowed violin strings. Acta
53 Acustica united with Acustica 44, 3 (1980) 194–206.
- 54 11. C. Maganza, R. Caussé, F. Laloë: Bifurcations, period
55 doublings and chaos in clarinetlike systems. Europhysics
56 Letters 1, 6 (1986) 295.
- 57 12. J.P. Dalmont, J. Gilbert, J. Kergomard: Reed instruments,
58 from small to large amplitude periodic oscillations and the
59 Helmholtz motion analogy. Acta Acustica united with
60 Acustica 86, 4 (2000) 671–684.
13. J. Gilbert, S. Maugeais, C. Vergez: Minimal blowing pressure
allowing periodic oscillations in a simplified reed musical
instrument model: Bouasse-Benade prescription assessed
through numerical continuation. Acta Acustica 4, 6 (2020) 27.
14. S. Terrien, C. Vergez, B. Fabre: Flute-like musical instruments:
a toy model investigated through numerical continuation.
Journal of Sound and Vibration 332, 15 (2013) 3833–3848.
15. R. Mattéoli, J. Gilbert, S. Terrien, J.-P. Dalmont, C. Vergez,
S. Maugeais, E. Brasseur: Diversity of ghost notes in tubas,
euphoniums and saxhorns. Acta Acustica 6 (2022) 32.
16. E. Gourc, C. Vergez, P.-O. Mattei, S. Missoum: Nonlinear
dynamics of the wolf tone production. Journal of Sound and
Vibration 516 (2022) 116463.
17. S. Terrien, R. Blandin, C. Vergez, B. Fabre: Regime change
thresholds in recorder-like instruments: influence of the
mouth pressure dynamics. Acta Acustica united with Acus-
tica 101, 2 (2015) 300–316.
18. S. Terrien, B. Bergeot, C. Vergez: Dynamic basins of
attraction in a toy-model of reed musical instruments, in:
Proceedings of Forum Acusticum, Turin, Italy, 11–15
September, 2023.
19. B. Bergeot, A. Almeida, C. Vergez, B. Gazengel: Measure-
ment of attack transients in a clarinet driven by a ramp-like
varying pressure. Proceedings of Acoustics, 2012.
20. B. Bergeot, A. Almeida, C. Vergez, B. Gazengel: Prediction
of the dynamic oscillation threshold in a clarinet model with
a linearly increasing blowing pressure. Nonlinear Dynamics
73 (2013) 521–534.
21. A. Ernout, B. Fabre: Temporal characterization of experi-
mental recorder attack transients. Journal of the Acoustical
Society of America 141, 1 (2017) 383–394.
22. S. Logie, S. Bilbao, J. Chick, M. Campbell: The influence of
transients on the perceived playability of brass instruments,
in: Proceedings of 20th International Symposium on Music
Acoustics, Sydney and Katoomba, 26–27 August, 2010.
23. K. Guettler, A. Askenfelt: Acceptance limits for the duration
of pre-Helmholtz transients in bowed string attacks. The
Journal of the Acoustical Society of America 101, 5 (1997)
2903–2913.
24. L. Velut, C. Vergez, J. Gilbert, M. Djahanbani: How well can
linear stability analysis predict the behaviour of an outward-
striking valve brass instrument model? Acta Acustica united
with Acustica 103, 1 (2017) 132–148.
25. A. Couineaux, F. Ablitzer, F. Gautier: Minimal physical
model of the cristal Baschet. Acta Acustica 7 (2023) 49.
26. B. Bergeot, S. Terrien, C. Vergez: Predicting transient
dynamics in a model of reed musical instrument with slowly
time-varying control parameter. Chaos: An Interdisciplinary
Journal of Nonlinear Science 34, 7 (2024) 073146.
27. T. Colinot, C. Vergez, P. Guillemain, J.-B. Doc: Multista-
bility of saxophone oscillation regimes and its influence on
sound production. Acta Acustica 5 (2021) 33.
28. M. Castellengo: Acoustical analysis of initial transients in
flute like instruments. Acta Acustica united with Acustica
85, 3 (1999) 387–400.
29. A. Almeida, R. Chow, J. Smith, J. Wolfe: The kinetics and
acoustics of fingering and note transitions on the flute.
Journal of the Acoustical Society of America 126, 3 (2009)
1521–1529.
30. A. Almeida, W. Li, E. Schubert, J. Smith, J. Wolfe:
Recording and analysing physical control variables used in
clarinet playing: A musical instrument performance capture
and analysis toolbox (MIPCAT). Frontiers in Signal Pro-
cessing 3 (2023) 1089366.

61
62
63
64
65
66
67
68
69
70
71
72
73
74
75
76
77
78
79
80
81
82
83
Q5 84
85
86
87
88
89
90
91
92
93
94
95
96
97
98
99
100
101
102
103
104
105
106
107
108
109
110
111
112
113
114
115
116
117
118
119
120
121
122
123
124

- 1 31. P.J. Menck, J. Heitzig, N. Marwan, J. Kurths: How basin
2 stability complements the linear-stability paradigm. *Nature*
3 *Physics* 9, 2 (2013) 89–92. 61
- 4 32. F. Silva, P. Guillemain, J. Kergomard, C. Vergez, V. Debut:
5 Some simulations of the effect of varying excitation param-
6 eters on the transients of reed instruments. *Proceedings of*
7 *Meetings on Acoustics* 19 (2013) 035058. 62
- 8 33. B. Cochelin, C. Vergez: A high order purely frequency-based
9 harmonic balance formulation for continuation of periodic
10 solutions. *Journal of Sound and Vibration* 324, 1–2 (2009)
11 243–262. 63
- 12 Q6 34. R. Bader: Musical instruments as synchronized systems, in:
13 R. Bader (ed.), *Springer handbook of systematic musicology*,
14 Springer, Berlin, Heidelberg, 2018, pp. 171–196 64
- 15 35. D. Dessi, F. Mastroddi, L. Morino: A fifth-order multiple-
16 scale solution for Hopf bifurcations. *Computers & Structures*
17 82, 31–32 (2004) 2723–2731. 65
- 18 36. T. Colinot, C. Vergez: How to build a MATLAB demon-
19 strator solving dynamical systems in real-time, with audio
20 output and MIDI control. *Acta Acustica* 7 (2023) 58. 66
- 21 37. L.F. Shampine, M.W. Reichelt: The matlab ode suite. *SIAM*
22 *Journal on Scientific Computing* 18, 1 (1997) 1–22. 67
- 23 38. S.H. Strogatz: *Nonlinear dynamics and chaos: with applica-*
24 *tions to physics, biology, chemistry, and engineering*,
25 Addison-Wesley Publication, Reading, MA, 1994. 68
- 26 39. A.H. Nayfeh, B. Balachandran: *Applied nonlinear dynamics:*
27 Q7 *analytical, computational, and experimental methods*, John
28 Wiley & Sons, 2008. 69
- 29 40. P. Schultz, P.J. Menck, J. Heitzig, J. Kurths: Potentials and
30 limits to basin stability estimation. *New Journal of Physics*
31 19, 2 (2017) 023005. 70
- 32 41. Y. Che, C. Cheng, Z. Liu, Z.J. Zhang: Fast basin stability
33 estimation for dynamic systems under large perturbations
34 with sequential support vector machine. *Physica D: Nonlinear*
35 *Phenomena* 405 (2020) 132381. 71
- 36 42. K. Siedenburg: Specifying the perceptual relevance of onset
37 transients for musical instrument identification. *Journal of*
38 *the Acoustical Society of America* 145, 2 (2019) 1078–1087. 72
- 39 43. K. Siedenburg, M.R. Schädler, D. Hülsmeier: Modeling the
40 onset advantage in musical instrument recognition. *Journal of*
41 *the Acoustical Society of America* 146, 6 (2019) EL523–EL529. 73
- 42 44. K. Siedenburg, S. McAdams: Four distinctions for the
43 auditory “wastebasket” of timbre. *Frontiers in Psychology* 8
44 (2017) 1747. 74
- 45 45. P.M. Galluzzo: *On the playability of stringed instruments*,
46 Q8 PhD thesis, University of Cambridge, 2004. 75
- 47 46. J.L. Hintze, R.D. Nelson: Violin plots: a box plot-density
48 trace synergism. *American Statistician* 52, 2 (1998) 181–184. 76
- 49 47. S. Weöglarczyk: Kernel density estimation and its applica-
50 tion. *ITM Web of Conferences* 23 (2018) 00037. 77
- 51 48. M. Stender, N. Hoffmann: bSTAB: an open-source software
52 for computing the basin stability of multi-stable dynamical
53 systems. *Nonlinear Dynamics* 107, 2 (2022) 1451–1468. 78
- 54 49. T. Bianco, V. Freour, I. Cossette, F. Bevilacqua, R. Caussé:
55 Measures of facial muscle activation, intra-oral pressure and
56 mouthpiece force in trumpet playing. *Journal of New Music*
57 *Research* 41, 1 (2012) 49–65. 79
- 58 50. B. Bergeot, C. Vergez: Analytical prediction of delayed Hopf
59 bifurcations in a simplified stochastic model of reed musical
60 instruments. *Nonlinear Dynamics* 107, 4 (2022) 3291–3312. 80
51. P. Brzeski, M. Lazarek, T. Kapitaniak, J. Kurths, P. Perlikowski: Basin stability approach for quantifying responses of multistable systems with parameters mismatch. *Meccanica* 51 (2016) 2713–2726. 61
52. C. Mitra, J. Kurths, R.V. Donner: An integrative quantifier of multistability in complex systems based on ecological resilience. *Scientific Reports* 5, 1 (2015) 16196. 62
53. M. Pàmies-Vilà, A. Hofmann, V. Chatziioannou: Analysis of tonguing and blowing actions during clarinet performance. *Frontiers in Psychology* 9 (2018) 617. 63
54. A. Lazarus, O. Thomas: A harmonic-based method for computing the stability of periodic solutions of dynamical systems. *Comptes Rendus Mécanique* 338, 9 (2010) 510–517. 64
55. L. Guillot, A. Lazarus, O. Thomas, C. Vergez, B. Cochelin: A purely frequency based Floquet-Hill formulation for the efficient stability computation of periodic solutions of ordinary differential systems. *Journal of Computational Physics* 416 (2020) 109477. 65

Appendix A

Trumpet model

We consider the brass instrument model described in [5]. The convention used to represent the lip position is given in Figure A1. The dimensioned and unregularized equations are as follows:

$$\begin{cases} \ddot{x} + \frac{\omega_L}{Q_L} \dot{x} + \omega_L^2(x - x_0) = \frac{p_0 - p}{\mu_L}, \\ \dot{p}_n - s_n p_n = Z_c C_n u \quad \forall n \in [1, N_m], \\ p = 2 \sum_{n=1}^{N_m} \Re(p_n), \\ u = W \sqrt{\frac{2|p_0 - p|}{\rho}} \cdot \text{sign}(p_0 - p) \cdot \max(x, 0), \end{cases} \quad (\text{A1})$$

with

$$\begin{cases} \omega_L = \sqrt{\frac{k}{m}}, \\ Q_L = \frac{\sqrt{km}}{c}, \\ \mu_L = \frac{m}{S}. \end{cases} \quad (\text{A2})$$

S is the surface area of the lip to which the pressures p_0 and p are applied, μ_L is the surface mass of the lip, Q_L its quality factor and ω_L its angular eigenfrequency. The resonator is represented by its input impedance, which is treated as a sum of N_m modes with poles s_n and residues C_n . The lip allows air to pass through a rectangular surface of height x and width W . The system equation (A1) is scaled as follows:

$$\begin{cases} \ddot{\tilde{x}} + \frac{\omega_L}{Q_L} \dot{\tilde{x}} + \omega_L^2(\tilde{x} - 1) = \omega_L^2(\gamma - \tilde{p}), \\ \dot{\tilde{p}}_n - s_n \tilde{p}_n = C_n \tilde{u} \quad \forall n \in [1, N_m], \\ \tilde{p} = 2 \sum_{n=1}^{N_m} \Re(\tilde{p}_n), \\ \tilde{u} = \zeta \sqrt{|\gamma - \tilde{p}|} \cdot \text{sign}(\gamma - \tilde{p}) \cdot \max(\tilde{x}, 0). \end{cases} \quad (\text{A3})$$

Variables affected by this scaling are marked with a symbol and are defined as follows:

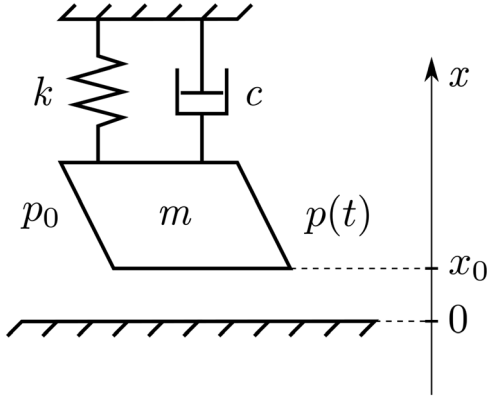


Figure A1. Schematic diagram of the one-degree-of-freedom lip model. Assume $x = 0$ when the lip is in the closed position and note x_0 the position of the lip at rest (the situation shown here).

Table A1. Resonator modal parameters. Complex residues C_n and poles s_n and resonance frequencies f_n .

n	C_n ($\text{kg} \cdot \text{s}^{-1} \cdot \text{m}^{-4}$)	s_n ($\text{rad} \cdot \text{s}^{-1}$)	f_n (Hz)
1	744.6	$-13.98 + i522.5$	83.15
2	954.5	$-22.42 + i1462$	232.7
3	1335	$-28.64 + i2187$	348.1
4	2582	$-37.64 + i2907$	462.6
5	3140	$-45.82 + i3658$	582.1
6	4191	$-49.82 + i4339$	690.6
7	4013	$-58.42 + i5029$	800.4
8	2602	$-66.77 + i5705$	908.1
9	1278	$-72.24 + i6459$	1028
10	909.7	$-94.40 + i7211$	1148
11	620.7	$-128.6 + i7931$	1262

$$\begin{cases}
 \tilde{x} = \frac{x}{x_0}, \\
 p_M = \mu_L \omega_L^2 x_0, \\
 \tilde{p} = \frac{p}{p_M}, \\
 \gamma = \frac{p_0}{p_M}, \\
 \tilde{p}_n = \frac{p_n}{p_M}, \\
 u_M = \frac{p_M}{Z_c}, \\
 \tilde{u} = \frac{u}{u_M}, \\
 \zeta = Z_c W x_0 \sqrt{\frac{2}{\rho p_M}}.
 \end{cases} \quad (\text{A4})$$

Irregular functions appearing in the flow term are regularized:

$$\begin{cases}
 |\bullet|_r = \sqrt{\bullet^2 + \epsilon}, \\
 \text{sign}(\bullet)_r = \frac{\bullet}{|\bullet|_r}, \\
 \max(\bullet, 0)_r = \frac{\bullet + |\bullet|_r}{2}.
 \end{cases} \quad (\text{A5})$$

The regularization term ϵ is arbitrarily set to $\epsilon = 10^{-6}$.

Time is scaled by the first modal angular frequency $\omega_1 = \Im(s_1)$ and the concerned variables are written with a symbol. Finally, we separate the real R_n and imaginary I_n parts of the modal pressures p_n , and the system we solve is as follows:

$$\begin{cases}
 \tilde{\ddot{x}} + \frac{\hat{\omega}_L}{Q_L} \tilde{\dot{x}} + \hat{\omega}_L^2 (\tilde{x} - 1) = \hat{\omega}_L^2 (\gamma - \tilde{p}), \\
 \hat{R}_n = \Re(\hat{s}_n) \hat{R}_n - \Im(\hat{s}_n) \hat{I}_n + \Re(\hat{C}_n) \tilde{u} \\
 \quad \forall n \in [1, N_m], \\
 \hat{I}_n = \Re(\hat{s}_n) \hat{I}_n + \Im(\hat{s}_n) \hat{R}_n + \Im(\hat{C}_n) \tilde{u} \\
 \quad \forall n \in [1, N_m], \\
 \tilde{p} = 2 \sum_{n=1}^{N_m} \Re(\tilde{p}_n), \\
 \tilde{u} = \zeta \sqrt{|\gamma - \tilde{p}|_r} \cdot \text{sign}(\gamma - \tilde{p})_r \cdot \max(\tilde{x}, 0)_r.
 \end{cases} \quad (\text{A6})$$

The parameter values chosen for this article are as follows:

$$\begin{cases}
 \omega_L = 2\pi \times 200 \text{ rad} \cdot \text{s}^{-1}, \\
 \mu_L = 2 \text{ kg} \cdot \text{m}^{-2}, \\
 Q_L = 3, \\
 x_0 = 1e - 4 \text{ m}, \\
 W = 8 \cdot 10^{-3} \text{ m}, \\
 Z_c = 1.83 \text{ kg} \cdot \text{s}^{-1} \cdot \text{m}^{-4}, \\
 \epsilon = 10^{-6}.
 \end{cases} \quad (\text{A7})$$

Appendix B

Modifications to bSTAB

The bSTAB toolbox [48] has been designed to calculate the basin stability of any dynamic system as automatically as possible. It generates initial conditions, performs a time integration for each of them, then classifies the obtained regime by comparing it to reference signals. In our case, we compare the peak-to-peak amplitude of R_2 , the real part of the second modal pressure, to that of the MANLAB solutions. Since classification must be performed on the steady part of the regime, the time integration continues until the following convergence criteria are met.

During the last duration t^* :

1. The amplitude of R_2 is within ϵ of that of a reference solution;
2. The difference between the amplitude of R_2 and that of the reference decreases.

The transient duration is defined as the duration after which the envelope of R_2 stays within ϵ of the amplitude of the reference solution. In this article, we choose $\epsilon = 0.1$.

The computation of the transient duration is illustrated in Figure B1a. The corresponding trajectory is also represented in Figure B1b, with its projection along x , R_2 and R_4 .

1

3
4
5
68
910
11
12
13
14
15

17

18
19
2022
2324
2526
27
28
29
30
31
32
33
3435
36
37
38
39
4041
42
43
44
45
46

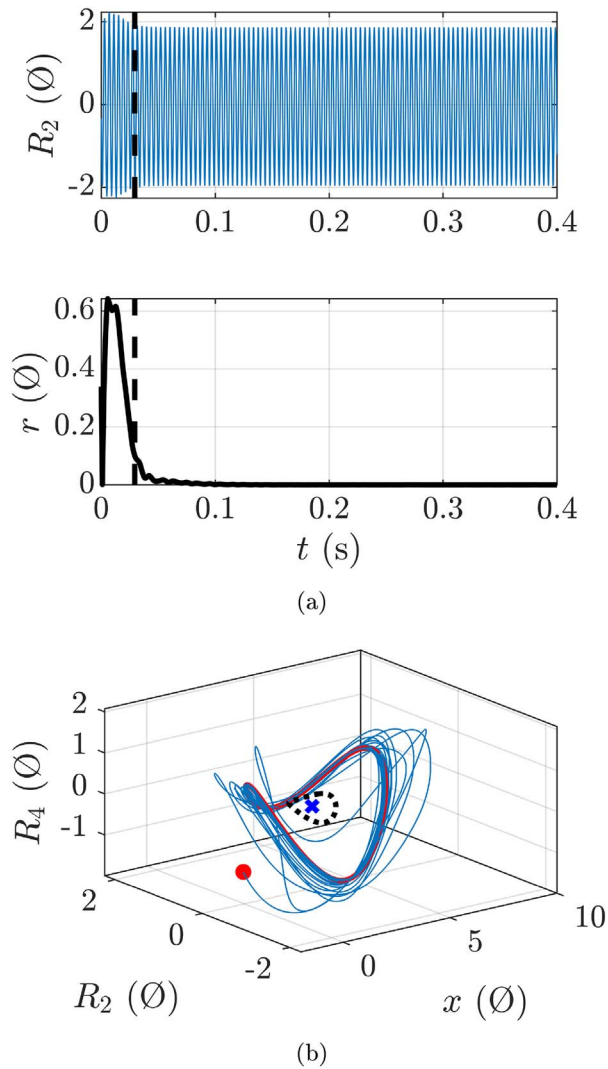


Figure B1. (a) Computation of the transient duration (represented by the dotted line) and (b) projection of the corresponding trajectory along x , R_2 and R_4 . The red dot is the initial state, the blue cross is the equilibrium, the red line is the stable periodic solution and the black broken line is the unstable periodic solution.

1
2

Cite this article as: Pégeot M. Colinot T. Doc J.-B. Fréour V. Vergez C, et al. 2024. Playability of self-sustained musical instrument models: statistical approaches. Acta Acustica, xx, xx. <https://doi.org/10.1051/aacus/2024075>.

EDP SCIENCES JOURNALS – AUTHOR QUERY FORM

Journal Code: aacus
Article Number: aacus240038
Article Title: Playability of self-sustained musical instrument models: statistical approaches

WARNING!

During the preparation of these proofs, your article was slightly modified, in particular to apply the AACUS typesetting policy.

Please carefully check for errors inadvertently introduced, in particular in:

- Title, author names, affiliation numbers and addresses, email addresses, ORCID IDs;
- Equations, units, figures, contents of Tables.

Regarding your proofs corrections:

- Any change concerning the scientific content (e.g. change of figure or of mathematical/physical values, addition of bibliographic references) will have to be approved by the Editor.
- If excessive changes to text or figures are requested, authors may be required to pay additional fees.
- Appendices are published as camera-ready material, i.e. kept as in your original manuscript. However, if you notice an error introduced during the production process, please let us know.

The author has the final responsibility for correcting the proofs.

Any correction received at another time will not be taken into account.

If the proofs are not returned within 5 days, publication of your paper will be delayed.

AUTHOR QUERIES – TO BE ANSWERED BY THE CORRESPONDING AUTHOR - MANDATORY

During the preparation of your manuscript for typesetting, the queries listed below have arisen.

Please answer each of these queries by adding the responses in this table, or by marking the corresponding corrections directly on this PDF file, or by writing your answers in the dedicated space on our platform, with your potential proofs corrections.

Query No.	Query/remark	Response
Q1	Please confirm that the meta-data of your article is correct: Title, author names, affiliation numbers, affiliations, email addresses, ORCID IDs.	
Q2	Please add complete address (street, city, state and postcode) in affiliations.	
Q3	Please add conflicts of interest statement.	
Q4	Please provide editor, publisher name and publisher location in reference [1].	
Q5	Please add conference location and date in reference [19, 22].	
Q6	Please check and approve the editor and publisher details added in reference [34].	
Q7	Please add publisher location in reference [39].	
Q8	Please add institution location in reference [45].	

Thank you for your assistance.
AACUS Production